Cytoplasmic keratins couple with and maintain nuclear envelope integrity in colonic epithelial cells

Carl-Gustaf A. Stenvall[a,†], Joel H. Nyström[a,†], Ciarán Butler-Hallissey[a,b,h], Theresia Jansson[a], Taina R. H. Heikkilä[a], Stephen A. Adam[c], Roland Foisner[d], Robert D. Goldman[c], Karen M. Ridge[c,e], and Diana M. Toivola[a,f,g,*]

[a]Cell Biology, Biosciences, Faculty of Science and Engineering, Åbo Akademi University, [b]Turku Bioscience Centre, University of Turku, and Åbo Akademi University, and [f]InFLAMES Research Flagship Center, Åbo Akademi University, 20500 Turku, Finland; [c]Department of Cell and Developmental Biology and [e]Pulmonary and Critical Care Medicine, Feinberg School of Medicine, Northwestern University, Chicago, IL 60611; [d]Max Perutz Labs, Medical University of Vienna, Vienna Biocenter Campus, 1030 Vienna, Austria; [g]Turku Center for Disease Modeling, University of Turku, 20520 Turku, Finland; [h]Aix Marseille Université, CNRS, INP UMR7051, NeuroCyto, 13005 Marseille, France

ABSTRACT **Keratin intermediate filaments convey mechanical stability and protection against stress to epithelial cells. Keratins are essential for colon health, as seen in keratin 8 knockout ($K8^{-/-}$) mice exhibiting a colitis phenotype. We hypothesized that keratins support the nuclear envelope and lamina in colonocytes. $K8^{-/-}$ colonocytes in vivo exhibit significantly decreased levels of lamins A/C, B1, and B2 in a colon-specific and cell-intrinsic manner. CRISPR/Cas9- or siRNA-mediated K8 knockdown in Caco-2 cells similarly decreased lamin levels, which recovered after reexpression of K8 following siRNA treatment. Nuclear area was not decreased, and roundness was only marginally increased in cells without K8. Down-regulation of K8 in adult $K8^{flox/flox}$;Villin-$CreER^{t2}$ mice following tamoxifen administration significantly decreased lamin levels at day 4 when K8 levels had reduced to 40%. K8 loss also led to reduced levels of plectin, LINC complex, and lamin-associated proteins. While keratins were not seen in the nucleoplasm without or with leptomycin B treatment, keratins were found intimately located at the nuclear envelope and complexed with SUN2 and lamin A. Furthermore, K8 loss in Caco-2 cells compromised nuclear membrane integrity basally and after shear stress. In conclusion, colonocyte K8 helps maintain nuclear envelope and lamina composition and contributes to nuclear integrity.**

Monitoring Editor
Thomas Magin
University of Leipzig

Received: Jun 18, 2020
Revised: Jul 20, 2022
Accepted: Aug 18, 2022

INTRODUCTION

Keratins (K) are the most abundant intermediate filament (IF) proteins and are divided into acidic type I keratins (K9–28) and basic/neutral type II keratins (K1–8 and K71–80; Schweizer *et al.*, 2006). Keratins form obligatory noncovalent heteropolymers in epithelial cells (Coulombe and Omary, 2002). The main simple epithelial keratins in the human colonic epithelium are K8 (type II), and K18, K19, and K20 (type I), with the additional type II K7 in mouse colon (Zhou *et al.*, 2003; Polari *et al.*, 2020). Keratins have multiple functions, including providing cell stress protection, mechanical stability, protein and organelle scaffolding, and modulating protein targeting in cells and tissues (Toivola *et al.*, 2005; Omary, 2017). Keratin mutations have been linked to several diseases in, for example, skin and liver,

This article was published online ahead of print in MBoC in Press (http://www.molbiolcell.org/cgi/doi/10.1091/mbc.E20-06-0387) on August 24, 2022.

†These authors contributed equally to this work.

Author contributions: C-G.A.S., J.H.N., K.M.R., C.B-H., T.J., S.A.A., R.D.G., and D.M.T. conceived and/or designed the experiments; C-G.A.S., J.H.N., C.B-H., T.R.H.H., T.J., K.R., and R.F. performed the experiments; C-G.A.S., J.H.N., C.B-H., T.R.H.H., and D.M.T. analyzed the data; C-G.A.S., J.H.N., and D.M.T. composed the manuscript; all authors edited the manuscript.

The authors declare no competing financial interest.

*Address correspondence to: Diana M. Toivola (diana.toivola@abo.fi).

Abbreviations used: IF, intermediate filament; INM, inner nuclear membrane; $K8^{-/-}$, K8 knockout mice $K8^{+/-}$, K8 heterozygote mice; $K8^{+/+}$, K8 wild type mice; K, keratins; LAP2α, lamina-associated polypeptide 2α; LINC complex, linker of nucleoskeleton and cytoskeleton complex; LMB, Leptomycin B; MEFs, mouse embryonic fibroblasts; ONM, outer nuclear membrane; pRb, retinoblastoma protein.

while their role in colon and inflammatory bowel diseases is under investigation (Coulombe *et al.*, 1991; Ku *et al.*, 2003; Toivola *et al.*, 2015; Omary, 2017). However, K8 knockout ($K8^{-/-}$) mice and mice with intestinal epithelium-specific K8 deletion ($K8^{flox/flox}$;Villin-Cre) display a colitis phenotype including epithelial erosion and hyperproliferation, disrupted barrier function, mild diarrhea, an ion-transport defect, deregulated epithelial differentiation, and blunted colonocyte energy metabolism (Baribault *et al.*, 1994; Toivola *et al.*, 2004; Helenius *et al.*, 2015; Asghar *et al.*, 2016; Lähdeniemi *et al.*, 2017; Stenvall *et al.*, 2021). $K8^{+/-}$ mice, which express 50% fewer keratins than $K8^{+/+}$ mice, exhibit an intermediate phenotype with moderate hyperproliferation, a partial ion transport defect, and increased susceptibility to experimental colitis, but no obvious spontaneous colitis under basal conditions (Asghar *et al.*, 2015, 2016; Liu *et al.*, 2017). Interestingly, $K8^{-/-}$ and $K8^{flox/flox}$;Villin-Cre mice in two models of colorectal cancer (Misiorek *et al.*, 2016; Stenvall *et al.*, 2021), and $K8^{+/-}$ mice in a model combining chemical colitis and colorectal cancer (Liu *et al.*, 2017), are highly susceptible to induced colorectal cancer. The colitis and hyperproliferation in $K8^{-/-}$ mice (Habtezion *et al.*, 2005) and the tumor load in $K8^{+/-}$ mice (Liu *et al.*, 2017) can be partly ameliorated with antibiotics, indicating that the microbiota plays a crucial part in these K8-deficient colon phenotypes.

The nuclear lamina is a filamentous meshwork beneath the inner nuclear membrane (INM) composed of type V IF proteins, the nuclear A- and B-type lamins, and INM proteins (Wilson and Foisner, 2010). A-type lamins, mainly lamins A and C, are encoded from the LMNA gene through alternative splicing. B-type lamins, primarily lamins B1 and B2, are encoded by the LMNB1 and LMNB2 genes, respectively (Dechat *et al.*, 2008). Lamins are important for many nuclear processes, including maintenance of nuclear morphology and integrity, mechanotransduction, chromatin organization, gene expression, differentiation, and proliferation (Dechat *et al.*, 2010; Wilson and Foisner, 2010; Naetar *et al.*, 2017; Brady *et al.*, 2018; de Leeuw *et al.*, 2018). These processes involve interactions between lamins and a multitude of lamin-binding proteins in the INM, nucleoplasm, and chromatin, including LAP2-Emerin-MAN1 (LEM)–domain proteins, lamin B receptor, and SUN proteins (Wagner and Krohne, 2007; Wilson and Foisner, 2010). For example, a nucleoplasmic LEM-domain protein, lamina-associated polypeptide 2α (LAP2α), is crucial for maintaining and regulating a pool of nucleoplasmic lamin A/C (Naetar *et al.*, 2008). LAP2α and nucleoplasmic lamin A/C interact with and promote the activity of the cell-cycle repressor retinoblastoma protein (pRb), thus controlling and inhibiting cell proliferation (Naetar *et al.*, 2008; Gesson *et al.*, 2014; Vidak *et al.*, 2018). Mutations in the lamin genes, mainly in the LMNA gene, cause many severe diseases termed laminopathies, such as Hutchinson-Gilford progeria syndrome, muscular dystrophies, and cardiomyopathies (Shin and Worman, 2022).

The nuclear lamina and the cytoskeleton are connected through LINC complexes, which are important for nuclear morphology, positioning, and mechanotransduction (Crisp *et al.*, 2006; Tapley and Starr, 2013; Osmanagic-Myers *et al.*, 2015). LINC complexes are composed of outer nuclear membrane (ONM) KASH proteins, including nesprins, connected to INM SUN proteins (Crisp *et al.*, 2006). The cytoskeleton binds LINC complexes either directly or through cytolinker proteins, such as plectin, and, for example, epidermal keratin IFs in keratinocytes and mesenchymal vimentin IFs are connected to nesprin-3 through plectin (Wilhelmsen *et al.*, 2005; Almeida *et al.*, 2015; Ketema *et al.*, 2013). Little is known about lamin and keratin synergy; however, epidermal K1/K10 loss has been linked to premature loss of nuclei, impaired nuclear integrity, and decreased lamin A/C, emerin, and SUN1 protein levels (Wallace *et al.*, 2012), and K14 loss in epidermal keratinocytes leads to aberrations in the shape and size of the nucleus (Lee *et al.*, 2012). Notably, the role of simple-type epithelial keratins in regulating nuclear lamin function, especially in the colonic epithelium, is unknown (Brady *et al.*, 2018). As we hypothesize that simple epithelial keratins may regulate lamins and the nucleus, this study aimed to assess whether the loss of these keratins affects lamins and lamin-associated proteins in $K8^{-/-}$ colonocytes. Here, we show that lamin protein levels correlate with simple epithelial keratin levels, particularly in colonocytes, and that cytoplasmic keratins contribute to maintaining nuclear envelope and lamina composition and provide support for nuclear integrity.

RESULTS

Loss of simple epithelial K8 correlates with decreased lamin levels in murine colonic epithelial cells in vivo

To determine whether simple epithelial keratins influence nuclear lamins in colonic epithelial cells, we analyzed lamin A, C, B1, and B2 levels as a function of keratin levels in colonic epithelial cells isolated from $K8^{+/+}$, $K8^{-/-}$ and $K8^{+/-}$ mice by Western blot analysis. The protein levels of lamins A, C, B1, and B2 in $K8^{-/-}$ mouse colonocytes were significantly decreased compared with $K8^{+/+}$ (Figure 1, A and B). $K8^{+/-}$ colonocytes also exhibited significantly decreased lamin B2 protein levels (twofold), but in contrast to $K8^{-/-}$, the decrease was moderate (Figure 1, A and B). In contrast, microarray analysis revealed a minor up-regulation of lamin A, B1, and B2 mRNA expression in $K8^{-/-}$ mouse colonocytes (Figure 1C). However, lamin gene expression analysis by quantitative reverse transcription PCR (qRT-PCR) showed that there was no significant change in lamin B1 mRNA levels, while lamin A/C and lamin B2 mRNA levels were decreased on average by 50% in $K8^{-/-}$ colonocytes compared with $K8^{+/+}$ (Figure 1D). Taken together, these data show that the protein levels of the major lamin isoforms A, C, B1, and B2 are decreased in $K8^{-/-}$ colonocytes and that the down-regulation is associated with decreased lamin gene expression, excluding lamin B1 mRNA.

Lamin down-regulation in the absence of K8 is specific for epithelial cells in the colon

To carefully define the location of the decreased lamin levels seen in the $K8^{-/-}$ colon, lamin A immunostaining was performed on $K8^{+/+}$ and $K8^{-/-}$ colon. $K8^{+/+}$ colonocytes express lamin A along the entire crypt, while clearly less lamin A was observed in the $K8^{-/-}$ crypt (Figure 2A). The weaker lamin signal could also be confirmed by measuring the fluorescence intensity of lamin A, which was approximately 35% less compared with $K8^{+/+}$ (Figure 2B). Intriguingly, the size of cell nuclei is comparable in $K8^{+/+}$ and $K8^{-/-}$ colonocytes (Figure 2, C and D), indicating that the decreased lamin protein levels are not caused by changes in nuclear size, while nuclear morphology analysis revealed that $K8^{-/-}$ nuclei are rounder than $K8^{+/+}$ nuclei (Figure 2E).

To assess whether lamins are affected in other epithelial tissues normally expressing K8 as a major type II keratin, lamin protein levels were analyzed in the small intestine (ileum), proximal colon, liver, pancreas, and lung (Supplemental Figure 1, A–F). In contrast to the $K8^{-/-}$ colon, the small intestine in $K8^{-/-}$ mice has a mild or negligible disease phenotype and does not display major hyperproliferation or inflammation (Baribault *et al.*, 1994; Ameen *et al.*, 2001). No changes in lamin A levels were observed in total lysates of $K8^{-/-}$ ileum, lungs, pancreas, and liver, while a decrease was seen in $K8^{-/-}$ proximal colon total lysates (Supplemental Figure 1, A–F). To determine

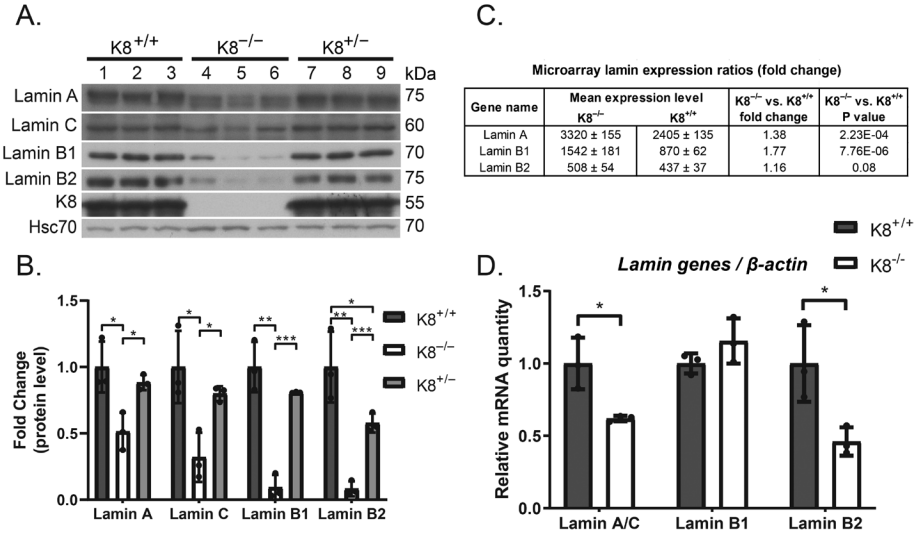

Gene name	Mean expression level $K8^{-/-}$	Mean expression level $K8^{+/+}$	$K8^{-/-}$ vs. $K8^{+/+}$ fold change	$K8^{-/-}$ vs. $K8^{+/+}$ P value
Lamin A	3320 ± 155	2405 ± 135	1.38	2.23E-04
Lamin B1	1542 ± 181	870 ± 62	1.77	7.76E-06
Lamin B2	508 ± 54	437 ± 37	1.16	0.08

FIGURE 1: Lamins A, C, B1, and B2 are down-regulated in isolated $K8^{-/-}$ mouse colon epithelial cells. (A) Lysates of crudely isolated colon epithelium from $K8^{+/+}$ (lanes 1–3), $K8^{-/-}$ (lanes 4–6), and $K8^{+/-}$ (lanes 7–9) mice ($n = 3$) were immunoblotted for lamin A, lamin C, lamin B1, lamin B2, and K8. Hsc70 was used as a loading control. (B) The immunoblots were quantified and normalized to Hsc70. The results are representative of two other similar sets of mice and represent the mean ($n = 3$) protein quantity ± SD with significant differences shown as * = $p < 0.05$, ** = $p < 0.01$, and *** = $p < 0.001$. (C) Lamin A, B1, and B2 mRNA levels in $K8^{+/+}$ $K8^{+/-}$ and $K8^{-/-}$ mouse colon were assessed by microarray analysis. (D) The mRNA levels of lamins A/C, B1, and B2 in $K8^{+/+}$ and $K8^{-/-}$ mouse colon total lysates were analyzed by qRT-PCR. The results were normalized to *β-tubulin* and represent the average ($n = 3$) fold change ± SD, with significant differences shown as * = $p < 0.05$.

Keratins maintain lamin levels in colorectal adenocarcinoma cells in vitro

To assess whether the effect of K8 down-regulation on colonocyte lamin levels in vivo is reproducible in vitro, human colorectal adenocarcinoma Caco-2 cells were subjected to sustained treatment with K8 and K18 siRNAs. Robust knockdown of keratins (about 80%) elicited a significant decrease in lamin A (about 40%) protein levels (Figure 3, A, C, and D). Immunofluorescence analysis of K8/K18 siRNA-treated cells revealed a similar decrease in lamin A levels (about 35%) in cells lacking K8/K18 (Supplemental Figure 3, A and B). Importantly, allowing siRNA-treated cells to recover for 9 days after siRNA treatment completely normalized K8/K18 protein levels (Figure 3, A–C), simultaneously rescuing the lamin A phenotype (Figure 3, B–D), indicating that lamin protein levels correlate with keratin levels in colon epithelial cells. Furthermore, a similar lamin phenotype manifested in $K8^{-/-}$ Caco-2 cells generated by CRISPR/Cas9-mediated gene knockout. $K8^{-/-}$ Caco-2 cells exhibited a complete loss of K8, K18, and K19 and a significant decrease in lamins A (about 50%), C (about 50%), and B2 (about 50%) protein levels compared with $K8^{+/+}$ CRISPR Caco-2 cells, while lamin B1 levels were unchanged (Figure 3, E and F). However, in contrast to our findings in vivo, $K8^{-/-}$ CRISPR Caco-2 cell nuclei are, on average, slightly larger than $K8^{+/+}$ nuclei, while nuclear morphology (roundness) is unchanged (Supplemental Figure 3, C–E).

whether the loss of other IF proteins may elicit a lamin phenotype, lamin protein levels were analyzed in $vimentin^{-/-}$ mouse spleen and colon, as $vimentin^{-/-}$ mice were recently found to be more sensitive to chemical colitis (Wang *et al.*, 2022). Western blot analysis revealed no changes in the levels of lamin A, C, B1, or B2 in $vimentin^{-/-}$ total colon and spleen lysates compared with $vimentin^{+/+}$ (Supplemental Figure 1, G–J). Taken together, these findings identify a colon- and colonocyte-specific role for keratins in the regulation of lamin protein levels.

The colitis and microbiota levels do not contribute to lamin down-regulation in $K8^{-/-}$ mouse colon

The colonic microbiota plays a crucial role in the $K8^{-/-}$ colon phenotype, as depletion of the colonic microbiota by broad-spectrum antibiotic treatment decreases inflammation and hyperproliferation in $K8^{-/-}$ mice (Habtezion *et al.*, 2005, 2011). Therefore, the impact of inflammation and microbiota on lamin protein expression was assessed in colonocytes from $K8^{+/+}$ and $K8^{-/-}$ mice treated with broad-spectrum antibiotics. Antibiotic treatment did not elicit any changes in, or normalization of, $K8^{-/-}$ colonocyte lamin protein levels compared with control (baseline) mice (Supplemental Figure 2, A and B). As seen by myeloperoxidase staining, decreased neutrophil infiltration in $K8^{-/-}$ colon confirmed that the antibiotic treatment ameliorated the inflammation in $K8^{-/-}$ colon (Supplemental Figure 2, C and D; Asghar *et al.*, 2015). Moreover, lamin A, B1, and C protein levels remained unchanged in mice treated with the colitis-inducing chemical dextran sodium sulfate (DSS) compared with untreated mice (Supplemental Figure 2, E and F). These findings exclude the colonic microbiota and the colitis observed in $K8^{-/-}$ colon as major contributing factors for the lamin changes and suggest a more direct role for keratins in the observed lamin phenotype.

The $K8^{-/-}$ colonocyte lamin phenotype manifests rapidly following the loss of K8

We next asked whether the loss of lamins in the keratin-deficient colon of the $K8^{-/-}$ mouse is colonocyte autonomous. For this, intestinal epithelium-specific $K8^{-/-}$ mice were established using the flox-Villin-Cre system. $K8^{flox/flox}$ mice were bred with either Villin-Cre or Villin-$CreEr^{t2}$ mice to generate K8 knockdown specifically in intestinal epithelial cells. $K8^{flox/flox}$;Villin-Cre mice are K8 deficient from birth, while the loss of K8 expression in $K8^{flox/flox}$;Villin-$CreER^{t2}$ mice is tamoxifen-inducible (one injection/day for 5 days, whereafter mice were sacrificed after 25 days). In both intestinal epithelium-specific $K8^{-/-}$ mouse models, lamin A and B1 protein levels were decreased in colonocytes (Figure 4, A–D), implying that this phenotype is indeed colonocyte-intrinsic. Next, we assessed at what time point the lamin phenotype manifests following sequential K8 loss over 14 days using tamoxifen-treated $K8^{flox/flox}$;Villin-$CreER^{t2}$ mice. While K8 protein levels on average started decreasing on day 1 after injection, the levels had decreased by 40% on day 4 and by ~90% on day 8 (Figure 4, E and F). A similar initial pattern was observed for lamins, with stable and significant down-regulation of lamin A and C protein levels starting 4–5 days after the first injection, while a down-regulation of lamin B2 was observed on day 8 and onward (Figure 4, E and F). Lamin A, C, and B2 protein levels were decreased by ~40% following K8 down-regulation. Lamin B1 protein levels were only reduced by ~20–30% starting from day 8 (Figure 4, E and F). Additionally, a minor lamin ratio shift was observed following K8 loss, with more prominent lamin B1 expression.

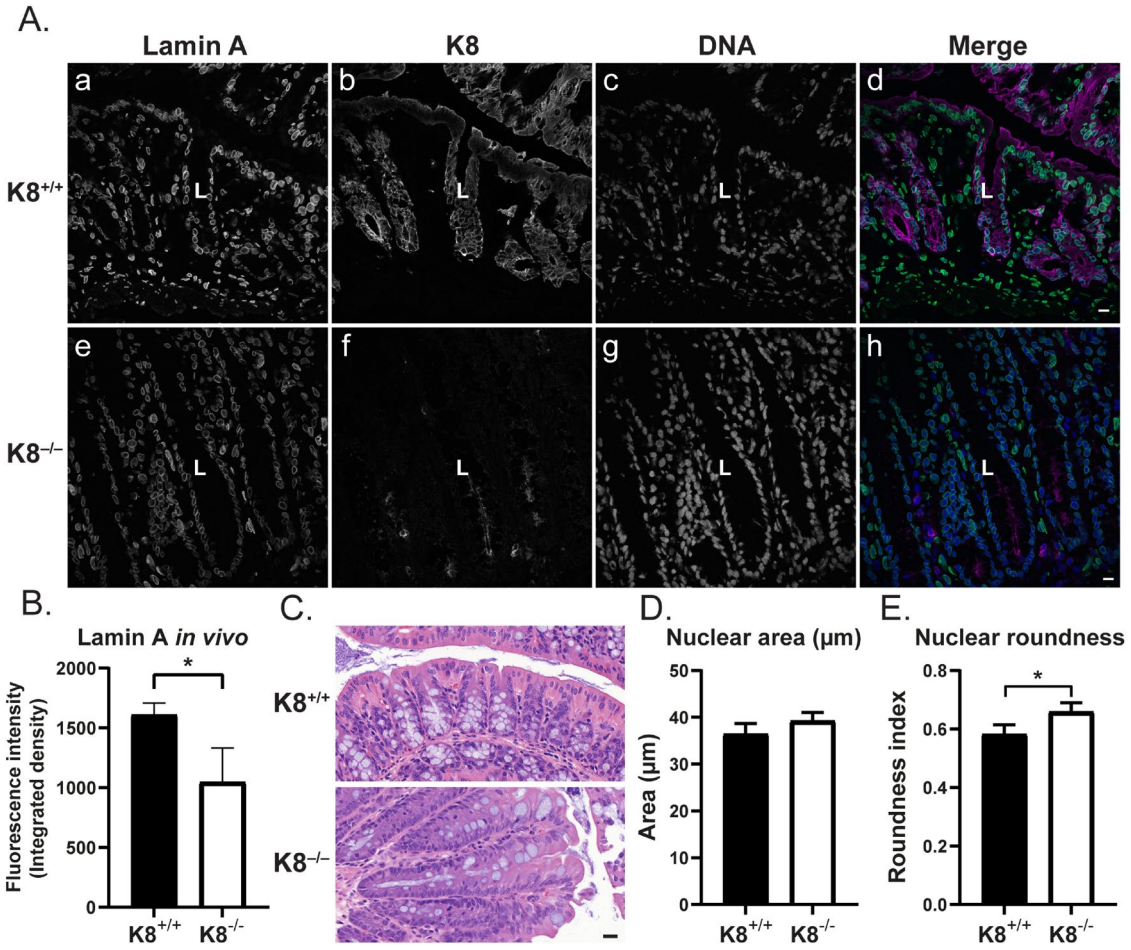

FIGURE 2: Loss of lamin A occurs only in K8$^{-/-}$ colon crypt epithelial cells. (A) K8$^{+/+}$ and K8$^{-/-}$ mouse colon tissue cryosections were immunostained for lamin A (green), K8 (magenta), and DNA (DRAQ5, blue). Scale bars = 25 µm. (B) Quantification of lamin A fluorescence intensity is shown in (A). The results represent the average fluorescence intensity per genotype (n = 33–132 cells analyzed/mouse, three mice analyzed/genotype) ± SD, with significant differences shown as * = $p < 0.05$. (C) Representative H&E images of K8$^{+/+}$ and K8$^{-/-}$ mouse colon tissue sections. (D, E) Analysis of nuclear area (D) and nuclear roundness (E) in K8$^{+/+}$ and K8$^{-/-}$ mouse colon tissue H&E images. The results represent the average nuclear size and nuclear roundness per genotype (n = 35–88 cells/per image; four images/mouse, four mice/genotype) ± SD, with significant differences shown as * = $p < 0.05$.

LINC complex protein levels are decreased in K8$^{-/-}$ mouse colonocytes, and SUN2 and lamin A complex with keratins

Loss of K1/K10 disrupts nuclear integrity and may decouple the cytoskeleton and nucleus in the epidermis (Wallace *et al.*, 2012). To assess whether nucleo-cytoskeletal coupling and nuclear integrity may also be connected to K8 in colonocytes, the levels of the cytolinker protein plectin and several LINC complex and lamin-associated proteins were assayed. K8$^{-/-}$ colonocytes exhibited reduced gene expression of SUN1, SUN2, and the INM protein emerin as seen by qRT-PCR, while no change was seen in plectin, nesprin-3, and LAP2α mRNA levels (Supplemental Figure 4A). SUN1, SUN2, and emerin protein levels were decreased in K8$^{-/-}$ colonocytes, and this down-regulation was larger than indicated by the qRT-PCR analysis, while plectin protein levels were significantly decreased (Figure 5, A and B). Out of this group of proteins, only emerin levels were moderately decreased in K8$^{+/-}$ colonocytes compared with K8$^{+/+}$ (Figure 5, A and B). Furthermore, similar to lamin A, SUN2 protein levels were unchanged in the small intestine (ileum) of K8$^{-/-}$ mice compared with K8$^{+/+}$, further indicating that there is no lamin phenotype in the small intestine (Supplemental Figure 4C). To assess whether the loss of SUN1 and SUN2 affects keratins and lamins, respectively, Caco-2 cells were treated with SUN1 and SUN2 siRNAs for 9 consecutive days (Supplemental Figure 4B). While keratins were unaffected by the loss of SUN1 and SUN2 proteins, lamin A protein levels were significantly reduced by approximately 25% (Supplemental Figure 4B). As keratins affect lamin and lamin-associated protein levels, we tested whether the reverse relationship occurs. Analysis of LAP2α$^{-/-}$ mice showed no change in either keratin or lamin protein levels in colonocytes (Supplemental Figure 4D). In addition, LAP2α is unchanged in K8$^{-/-}$ mouse colonocytes (Supplemental Figure 4E). This suggests that the complex containing lamin A/C, LAP2α and pRb is downstream from keratin-lamin interaction (Naetar *et al.*, 2008; Stenvall *et al.*, 2021), and hence, loss of LAP2α does not alter keratin protein levels. To understand any molecular connection between keratins and nuclear lamins, K8/K18 or lamin A co-immunoprecipitation assays were performed on lysates of Caco-2 cells. K8/K18 co-immunoprecipitated with lamin A and the LINC complex protein SUN2 and, conversely, lamin A coimmunoprecipitated K8, K18, and K19 (Figure 5, C and D).

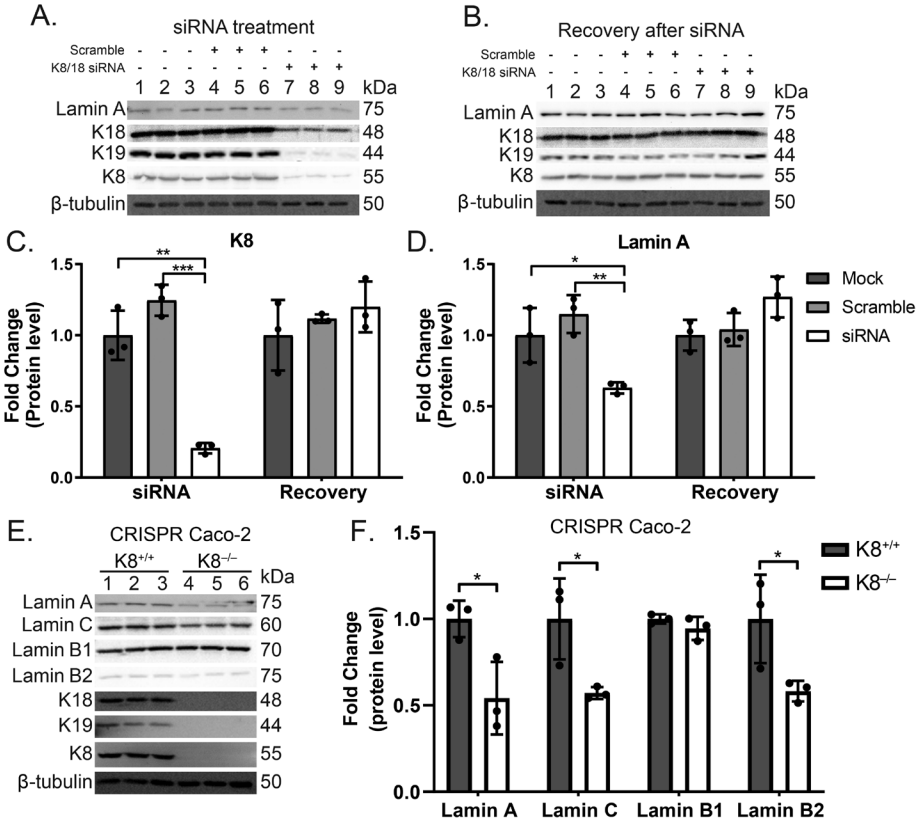

FIGURE 3: Caco-2 cells without keratins exhibit reduced lamin protein levels, which can be rescued by re-expression of keratins. (A) Mock-transfected (all reagents except siRNA), K8/K18 scramble siRNA-transfected, and K8/K18 siRNA-transfected Caco-2 cells were immunoblotted for lamin A, K8, K18, and K19. β-tubulin was used as a loading control. (B) Cells were allowed to recover after siRNA treatment and analyzed by immunoblotting for lamin A, K8, K18, and K19. β-tubulin was used as a loading control. Recovery of the cells after siRNA treatment led to reexpression of keratins and rescue of lamin expression. (C, D) The immunoblots in A and B were quantified and normalized to β-tubulin and represent the mean ($n = 3$) protein quantity ± SD with significant differences shown as * = $p < 0.05$, ** = $p < 0.01$, and *** = $p < 0.001$. (E) CRISPR/Cas-9 K8$^{-/-}$ Caco-2 cells were immunoblotted for lamin A, lamin C, lamin B1, lamin B2, K18, K19, and K8. β-tubulin was used as a loading control. (F) The lamin immunoblots in E were quantified and normalized to β-tubulin. The results represent the mean ($n = 3$) protein quantity ± SD with significant differences shown as * = $p < 0.05$.

K8 is not detected in colonocyte nuclei

As low levels of nuclear keratins have been reported in HeLa cells (Kumeta *et al.*, 2013), we analyzed whether keratins may be present in colonocyte nuclei. Airyscan microscopy of Caco-2 cells immunostained for K8 and lamin A revealed that keratins and lamins are in close proximity at the nuclear surface, while no nucleoplasmic keratins were observed (Figure 5F and Supplemental Videos 1–3). Furthermore, treatment of Caco-2 cells with the nuclear export inhibitor leptomycin B (LMB) did not cause any detectable accumulation of keratins in the nucleus (Supplemental Figure 5A and Supplemental Videos 2 and 3). In contrast, nuclear accumulation of the positive control pRb was increased after LMB treatment (Supplemental Figure 5, B and C). Similarly, no nuclear K8 was detected in vivo in mouse colon sections after overexposure of the abundant cytoplasmic keratin filaments (Figure 5E). Together, these data indicate that cytoplasmic keratins can complex with LINC complex components and lamins, suggesting that keratins could physically link to the lamina via the LINC complex and may thus affect the mechanical properties of the nucleus, and thereby modulate nuclear function.

Nuclear integrity is compromised following K8 loss in colorectal adenocarcinoma cells, and is further exacerbated by shear stress

The nuclear lamina and the functional coupling of the cytoskeleton and nucleus are important for nuclear integrity. Because the levels of many LINC complex and nuclear lamina components are decreased in K8$^{-/-}$ colonocytes, we assessed whether nuclear integrity is affected following the loss of K8 by transfecting cells with NLS-GFP or cGAS-RFP, which are contained in the nucleus when the nuclear lamina is intact (Figure 6, A and C; Denais *et al.*, 2016; Jiang *et al.*, 2019). K8$^{-/-}$ CRISPR Caco-2 cells showed a significant threefold increase in the percentage of transfected cells with cytoplasmic NLS-GFP compared with K8$^{+/+}$ cells (Figure 6B). Exposure to shear stress for 24 hours in an orbital shaker, which increased K8$^{+/+}$ nuclear leakage of NLS-GFP, further increased the number of K8$^{-/-}$ CRISPR Caco-2 cells with NLS-GFP in the cytoplasm (Figure 6B). A similar threefold increase in baseline nuclear leakiness was seen for K8$^{-/-}$ CRISPR Caco-2 cells transfected with cGAS-RFP compared with K8$^{+/+}$ cells, while shear stress did not further increase the number of cells with cytoplasmic cGAS-RFP (Figure 6D). Taken together, the loss of K8 leads to a compromised nuclear envelope in colorectal cancer cells.

DISCUSSION

In this study, we demonstrate a molecular link between cytoplasmic simple epithelial keratins, LINC complex proteins, lamin-associated proteins, and nuclear lamins, especially in colonocytes (summarized in Figure 7). We show that the absence of keratins in colon epithelial cells leads to significantly decreased protein levels of the major lamin isoforms A, C, B1, and B2 in vivo in adult full-body K8$^{-/-}$ mice, and in two models where K8 was deleted only from intestinal epithelial cells (K8$^{flox/flox}$;Villin-Cre mice, and after tamoxifen administration to K8$^{flox/flox}$;Villin-CreER^{t2} mice). Similarly, lamin protein levels decrease in vitro in human Caco-2 cells treated with K8/K18 siRNA or in CRISPR/Cas9 K8$^{-/-}$ Caco-2 cells. Reduced lamin gene expression, except for lamin B1, is likely in part the cause of the decreased lamin protein levels observed in K8$^{-/-}$ colon; however, it is unclear how the loss of keratins could affect lamin expression, as little is known about lamin gene regulation (Dechat *et al.*, 2008). Matrix stiffness and the vitamin A/retinoic acid pathway have been implicated in lamin A transcriptional regulation (Swift *et al.*, 2013). Furthermore, the gene Hey regulates the *Drosophila* A-type lamin C and B-type lamin Dm$_0$ genes. The loss of Hey is linked to increased lamin Dm$_0$ and decreased lamin C expression in differentiated *Drosophila* enterocytes (Flint Brodsly *et al.*, 2019). This is intriguing as murine Hey1 and Hey2 are down-regulated in K8$^{-/-}$ colonocytes (Lähdeniemi *et al.*, 2017), suggesting that Hey1 and Hey2 may be involved in colonocyte lamin gene regulation. The concomitant changes in K8 and lamin levels also occur in an acute setting

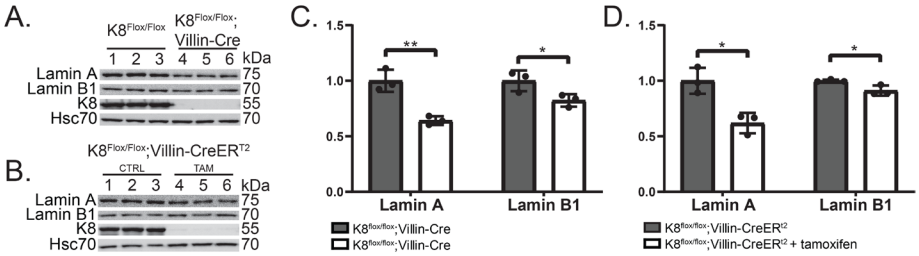

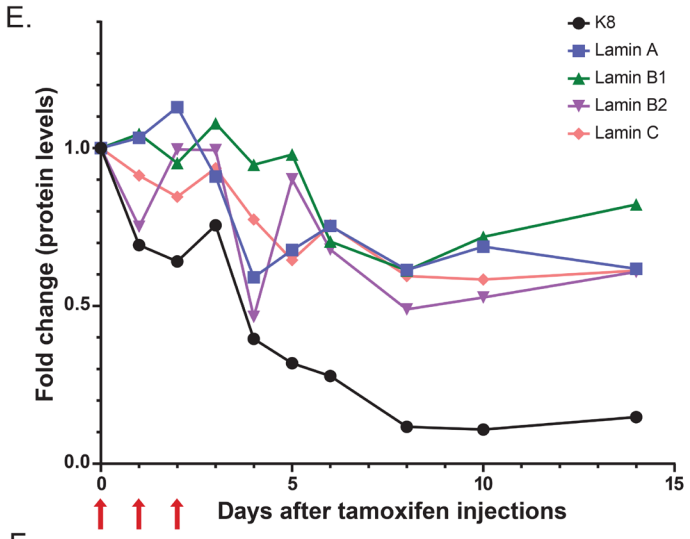

F.

Days (*)	1	2	3	4	5	6	8	10	14
K8	0.23	0.03	0.04	0.13	0.05	0.01	0.15	0.06	0.17
Lamin A	0.21	0.07	0.17	0.17	0.09	0.11	0.13	0.07	0.13
Lamin C	0.11	0.13	0.08	0.16	0.04	0.01	0.01	0.06	0.12
Lamin B1	0.18	0.08	0.15	0.06	0.13	0.01	0.14	0.04	0.05
Lamin B2	0.19	0.05	0.09	0.27	0.22	0.24	0.09	0.03	0.14

* days after tamoxifen injection; statistical significance = n.s. | p < 0.05 | p < 0.01 | p < 0.001
Numbers in boxes indicate SD for the individual days with n=3

FIGURE 4: Lamin protein down-regulation occurs rapidly following loss of K8 expression. (A) Lysates of crudely isolated colon epithelium from control K8$^{flox/flox}$ (lanes 1–3) and K8$^{flox/flox}$;Villin-Cre (endogenous K8 knockdown, lanes 4–6) mice and (B) untreated K8$^{flox/flox}$;Villin-CreER^{t2} (lanes 1–3) and tamoxifen-treated K8$^{flox/flox}$;Villin-CreER^{t2} (induced K8 knockdown, lanes 4–6) mice were immunoblotted for lamin A, lamin B1, and K8. Hsc70 was used as a loading control. (C, D) The immunoblots were quantified and normalized to Hsc70 protein levels and the results represent the mean ($n = 3$) protein quantity ± SD with significant differences shown as * = $p < 0.05$ and ** = $p < 0.01$. (E) K8$^{flox/flox}$;Villin-CreER^{t2} were sacrificed at different time points ($n = 3$ per time point) after tamoxifen injections and lysates of crudely isolated colon epithelium were obtained and immunoblotted and quantified for lamin A, lamin C, lamin B1, lamin B2, and K8. Hsc70 was used as a loading control. Arrows show days of tamoxifen injection. (F) Quantification of daily changes in protein levels by comparison to day 0, with significant differences shown with the colors light blue = $p < 0.05$, blue = $p < 0.01$, and dark blue = $p < 0.001$, and SD for individual days shown as numbers in boxes.

and are closely linked temporally. Lamin levels are also normalized when K8 is allowed to be reexpressed in Caco-2 cell cultures after siRNA treatment. In vivo, reducing intestinal epithelial K8 levels stepwise by treating adult K8$^{flox/flox}$;Villin-CreER^{t2} mice with tamoxifen, leads to a 60% drop in colonic K8 protein levels that is accompanied by statistically significant decreases in lamin A and B2 protein levels within 4 d.

Interestingly, the decrease in lamin protein levels was observed only in the epithelium of the colon, as several other K8$^{-/-}$ simple epithelial tissues, in which K8 is also a major (or the only) type II keratin, exhibited normal lamin and SUN2 protein levels as assessed for, amongst others, the small intestine. Furthermore, no changes in lamin protein levels were observed in the spleen or colon of vimentin$^{-/-}$ mice, suggesting this is a keratin-specific effect. The correlation between keratin loss and decreased lamin levels is likely independent of the microbiota or colitis observed in K8$^{-/-}$ mice, as antibiotic treatment, which eliminates the colonic microbiota and ameliorates colitis and hyperproliferation (Habtezion *et al.*, 2011), did not normalize lamin levels. However, as the effect of keratin loss on lamin levels is not universal for keratin-expressing epithelia or other intermediate filament proteins, we cannot rule out that colon epithelium-specific functions and processes are involved in this regulation. Very little is known regarding the potential roles of lamins in colon homeostasis and function (Brady *et al.*, 2018). Low levels of A-type lamins correlate with increased gastric polyp size (Wang *et al.*, 2015), and loss of A-type lamins in stage II and III colorectal cancers (CRCs) puts patients at severe risk of cancer resurgence (Belt *et al.*, 2011). Because the lack or decreased levels of colonic keratins leads to hyperproliferation and increased susceptibility to CRC tumorigenesis (Misiorek *et al.*, 2016; Liu *et al.*, 2017; Lähdeniemi *et al.*, 2017; Stenvall *et al.*, 2021), the lamin phenotype in these mice may be a contributing factor toward the pro-proliferative and pro-tumorigenic phenotype. Nevertheless, mouse intestinal epithelial-specific lamin A knockdown in mice did not lead to increased proliferation as measured by KI67 (Wang *et al.*, 2015).

Lamin-associated proteins depend on A-type lamins, and vice versa, for stabilization and correct positioning in the nucleus (Vaughan *et al.*, 2001; Libotte *et al.*, 2005; Naetar *et al.*, 2008; Muchir *et al.*, 2009). Our data show that K8$^{-/-}$ mouse colonocytes have decreased levels of emerin, which is anchored to the INM by lamin A, and therefore the absence of emerin could be caused by decreased lamin A protein levels (Vaughan *et al.*, 2001; Muchir *et al.*, 2009). Weakening or loss of the connection between the nuclear lamina and the cytoplasmic cytoskeleton can be caused by the loss and/or mislocalization of lamins and/or LINC complex proteins, leading to the loss of anchoring sites for connecting the nuclear lamina to LINC complexes (Lombardi and Lammerding, 2011). As several LINC complex proteins, including SUN1 and SUN2, and the major lamin isoforms are down-regulated in K8$^{-/-}$ colonocytes, we can surmise that the coupling of LINC complexes and the nuclear lamina may be compromised in these cells. While we could not probe nesprin-3 protein levels due to the lack of a suitable antibody, nesprin-3 gene expression was unaffected in K8$^{-/-}$ colonocytes. Nonetheless, as SUN proteins are required for the correct localization of nesprin-3 at the ONM (Ketema *et al.*, 2007), and SUN1 and SUN2 are down-regulated in K8$^{-/-}$ colonocytes, nesprin-3 is

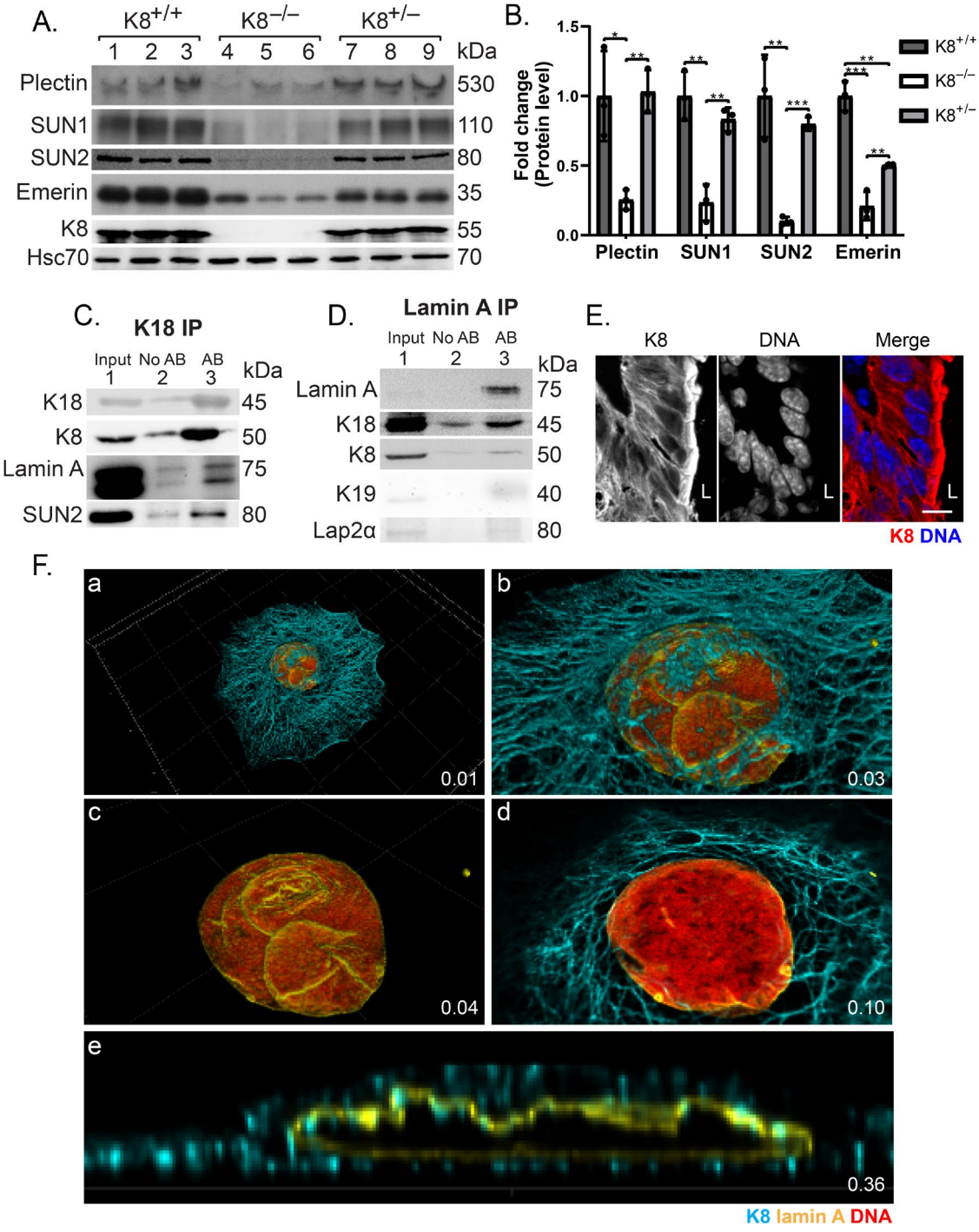

FIGURE 5: LINC complex protein levels are decreased in K8$^{-/-}$ colon epithelial cells. (A) Lysates of crudely isolated colon epithelium from K8$^{+/+}$ (lanes 1–3), K8$^{-/-}$ (lanes 4–6), and K8$^{+/-}$ (lanes 7–9) mice ($n = 3$) were immunoblotted for plectin, SUN1, SUN2, emerin, and K8. Hsc70 was used as a loading control. (B) The immunoblots were quantified and normalized to Hsc70 and represent the mean ($n = 3$) protein quantity ± SD with significant differences shown as * = $p <$ 0.05, ** = $p < 0.01$, and *** = $p < 0.001$. (C, D) Caco-2 cell lysates (input) were used in immunoprecipitation assays where K8/K18 (C) or lamin A (D) were immunoprecipitated using K18 or lamin A antibodies, respectively. The immunoprecipitates were immunoblotted for K8, K18, K19, lamin A, SUN2, and LAP2α. K8/K18 co-immunoprecipitated lamin A and SUN2, and lamin A co-immunoprecipitated K8, K18, K19, and LAP2α. No AB indicates a negative control sample, in which the immunoprecipitation step was performed without antibody. (E) K8$^{+/+}$ mouse colon tissue cryosections were immunostained for K8 (red) and DNA (DRAQ5, blue). Scale bar = 10 μm; L = lumen. (F) 3D rendering of Caco-2 cells immunostained for DNA (red), lamin A (yellow), and K8 (cyan). The time points from Supplemental video 1 are listed for each individual image.

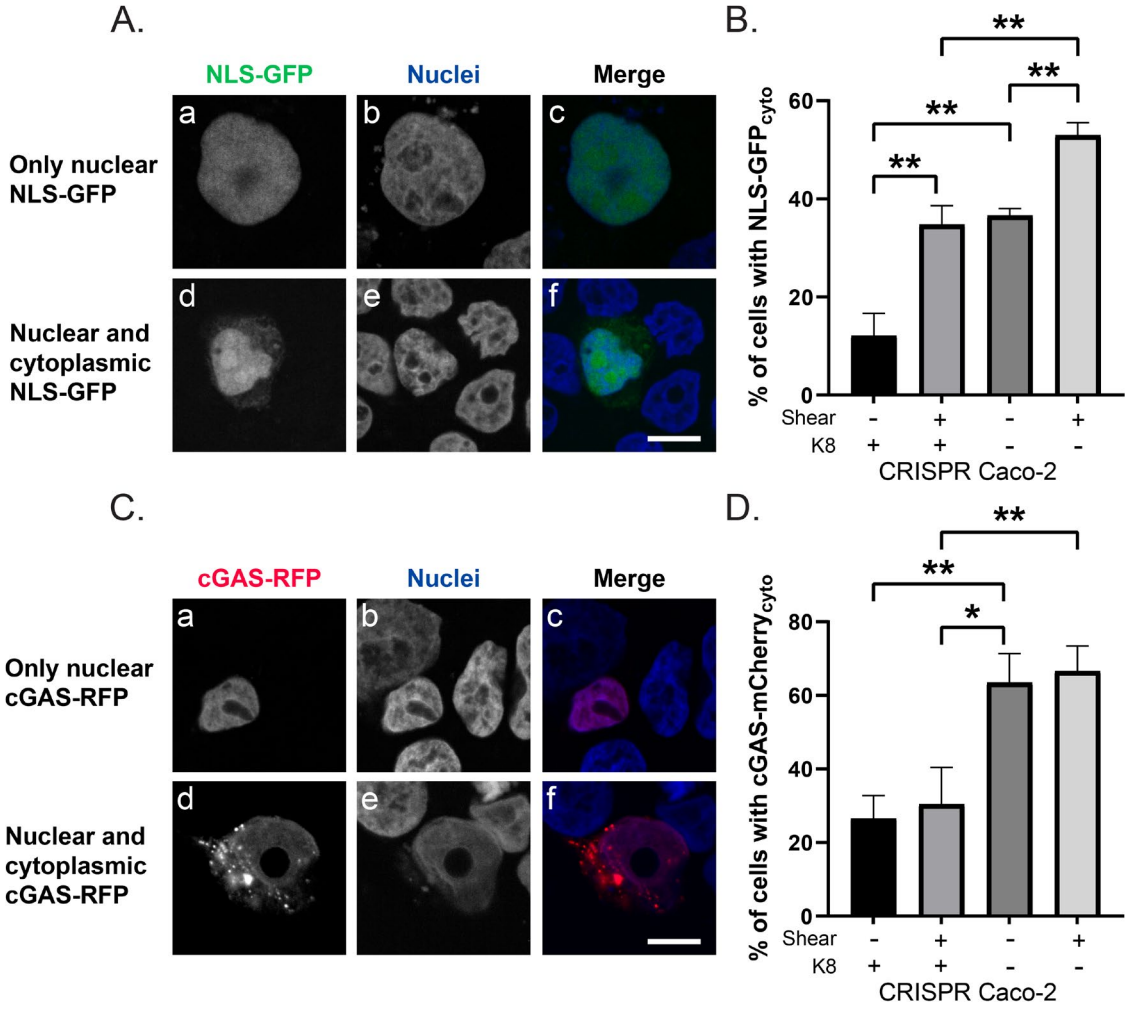

FIGURE 6: Nuclear integrity is compromised in K8$^{-/-}$ Caco-2 cells. (A, C) CRISPR/Cas-9 K8$^{+/+}$ and K8$^{-/-}$ Caco-2 cells were transfected with NLS-GFP and cGAS-RFP and were subjected to shear stress in an orbital shaker (± shear) or used as static controls (± K8). Representative images of cells with either nuclear or both nuclear and cytoplasmic NLS-GFP (green) and cGAS-RFP (red) are shown. Nuclei are visualized with DAPI (blue). (B, D) The number of cells with only nuclear or with both nuclear and cytoplasmic NLS-GFP and cGAS-RFP in cells was quantified. The results represent the average of two data sets (10–15 images analyzed/condition/data set) ± SD, with significant differences shown as * = $p < 0.05$ and ** = $p < 0.01$.

presumably displaced from the ONM. Furthermore, plectin, a cytolinker protein known to link nesprin-3 to vimentin and keratins (Wilhelmsen *et al.*, 2005; Ketema *et al.*, 2013; Almeida *et al.*, 2015), is decreased in K8$^{-/-}$ colonocytes, which supports the notion that the nucleoskeleton–cytoskeleton link is disrupted from the outside of the nucleus due to the loss of keratins and plectin. Our data in colonocytes support the findings reported for other cell types, that a continuous coupling between the cytoplasmic cytoskeleton and the nuclear lamina and the presence of lamins and lamin-associated proteins, such as emerin, are essential for maintaining nuclear integrity and mechanosignaling (Lombardi and Lammerding, 2011; Osmanagic-Myers *et al.*, 2015; Chen *et al.*, 2018).

Due to the decrease of many proteins along the axis spanning the keratin cytoskeleton, LINC complexes, and the nuclear lamina, we hypothesized that nuclear integrity and mechanosignaling are weakened or disrupted in K8$^{-/-}$ colonocytes, and that nuclei in these cells are more vulnerable to mechanical stress. Indeed, Caco-2 cells lacking K8 exhibit more nuclear membrane ruptures and are more susceptible to shear stress than wild-type cells, indicating that the loss of K8 leads to disruption of nuclear integrity. This is supported by the findings that epidermal K1/K10 loss in mice is associated with decreased levels of lamin A/C, emerin, and SUN1 and a likely decoupling of the cytoskeleton and the nuclear lamina, leading to weakened nuclear integrity and premature loss of nuclei (Wallace *et al.*, 2012). Similarly, the loss of vimentin in mouse embryonic fibroblasts (MEFs) causes increased nuclear rupture and DNA damage during cell migration (Patteson *et al.*, 2019). In addition, MEFs lacking all nuclear lamins display nuclear membrane ruptures, the frequency of which increases even further following mechanical stress, while the frequency of ruptures is reduced following disruption of cytoskeletal forces (Chen *et al.*, 2018). It is plausible that the weakened nuclear integrity in K8$^{-/-}$ colonocytes is caused by a combination of events. For example, as K8$^{-/-}$ colonocyte nuclei are not protected by an intact keratin network (Almeida *et al.*, 2015), and likely have weaker nuclear envelopes as a consequence of reduced lamin levels (Chen *et al.*, 2018), they are more prone to nuclear envelope rupturing following exposure to compressive forces in the colon (e.g., peristalsis) and to the

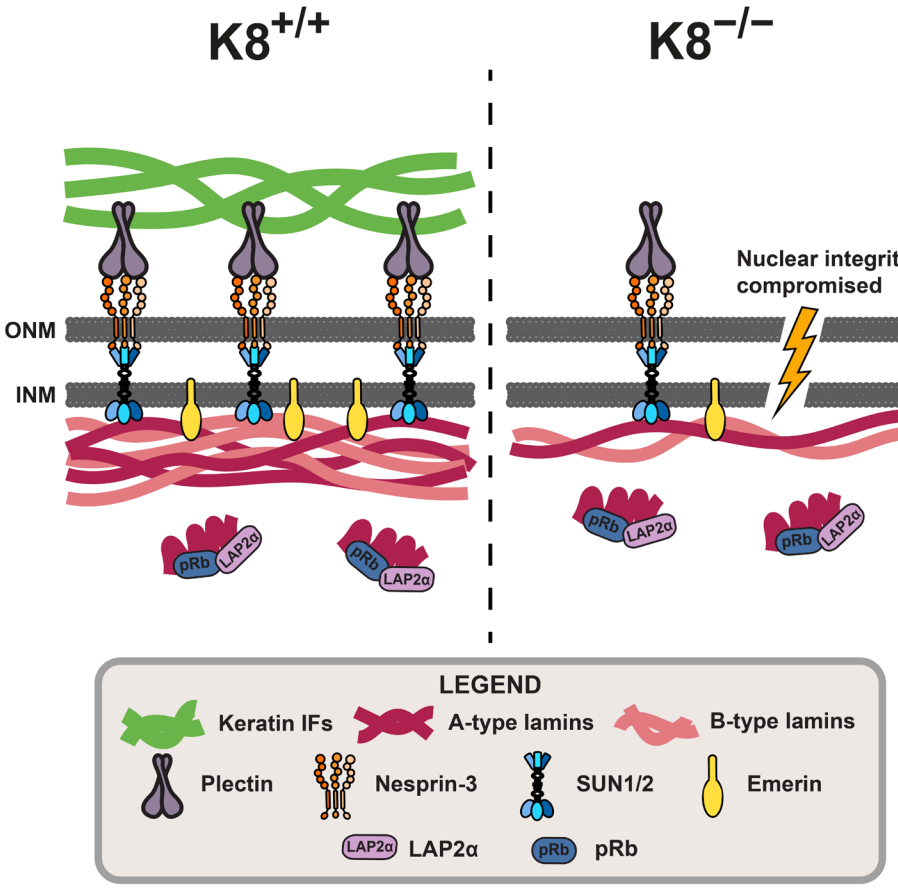

FIGURE 7: In this summary schematic, the findings of this study are summarized. In healthy colon epithelial cells ($K8^{+/+}$), cytoplasmic K8-containing keratin IFs couple with and/or stabilize plectin, LINC complex proteins, lamins, and lamin-associated proteins, thus helping maintain nucleocytoskeletal coupling, nuclear envelope and lamina composition, nuclear integrity, and nuclear function. Loss of cytoplasmic keratins ($K8^{-/-}$) in colon epithelial cells correlates with decreased plectin, LINC complex, lamin, and lamin-associated protein levels, which likely disrupts these nuclear membrane complexes and compromises nuclear integrity.

pushing and pulling forces of active colonocyte migration (Krndija *et al.*, 2019). Furthermore, shear stress in lung alveolar cells has been shown to induce K8 phosphorylation and changes in filament assembly, which might also play a role in colonocyte K8 dynamics during mechanical stress conditions (Ridge *et al.*, 2005; Flitney *et al.*, 2009; Sivaramakrishnan *et al.*, 2009).

In a similar vein, cytoskeletal, LINC complex, and lamin proteins are determinants of nuclear size and shape. Nuclear size is reduced and nuclei are more elongated in K14-deficient mouse epidermis (Lee *et al.*, 2012), while depletion of desmin or its ONM binding partner nesprin-3 causes nuclear collapse in rat cardiomyocytes (Heffler *et al.*, 2020). Furthermore, Vahabikashi and colleagues have shown that lamin B2-deficient MEF nuclei are similar in size to wild-type nuclei, while lamin B1-deficient MEF nuclei are smaller and lamin A/C-, lamin A-, and lamin C-deficient MEF nuclei are larger than in wild-type MEFs (Vahabikashi *et al.*, 2022). While the disruption of different lamin isoforms had a variety of effects on nuclear size, all lamin-deficient MEFs exhibited rounder nuclei (Vahabikashi *et al.*, 2022). Interestingly, in contrast to the reduced nuclear size in K14-deficient epidermis and desmin-deficient cardiomyocytes (Lee *et al.*, 2012; Heffler *et al.*, 2020), K8 loss did not elicit a change in nuclear size in colonocytes, while the nuclei in $K8^{-/-}$ CRISPR Caco-2 cells were slightly larger than their wild-type counterparts. Consequently, this excludes the possibility that the reduced lamin protein levels in $K8^{-/-}$ colonocytes would have been a consequence of smaller nuclei. The rounder $K8^{-/-}$ colonocyte nuclei could reflect the loss of cytoskeletal/contractile forces that maintain nuclear shape. Taken together, our data and these published studies highlight a clear role for cytoplasmic and nuclear IF proteins in nuclear morphology and function, while the effects are likely cell and tissue type-specific.

Recent intriguing studies have described the presence of low levels of traditionally cytoplasmic keratins inside the nucleus, where they can modulate several signaling pathways (Kumeta *et al.*, 2013; Escobar-Hoyos *et al.*, 2015; Hobbs *et al.*, 2015; Jacob *et al.*, 2020). We were, however, unable to detect any nuclear K8 basally in vivo or following LMB treatment of Caco-2 cells. Our 3D cell analysis did, on the other hand, reveal that K8 and lamins are found to be located intimately together by the nuclear membrane, and that it is likely that they complex, as shown by our co-immunoprecipitation analysis, at this location. While we have been unable to elucidate more detailed spatial information on these complexes and where exactly K8 may bind to and interact with the nuclear envelope and its components, our data opens up intriguing new avenues of research regarding how keratins and other IFs may interact with cell nuclei.

In conclusion, we show in this study that simple epithelial keratin filaments offer support to lamins, LINC complex proteins, and lamin-associated proteins in colonic epithelial cells, and that K8 loss leads to dramatically decreased levels of these proteins. Consequently, the coupling between the cytoskeleton and nuclear lamina is disrupted and nuclear integrity is compromised. Our findings indicate a novel, colonocyte-specific role for K8 in maintaining nuclear envelope and lamina composition, nuclear integrity and nuclear function, and that K8 may be a novel cytoskeletal factor involved in the mechanical coupling of the cytoskeleton and the nucleus.

MATERIALS AND METHODS

Experimental animals and sample collection

$K8^{+/+}$, $K8^{+/-}$, and $K8^{-/-}$ mice in the FVB/n background (Baribault *et al.*, 1994) and $K8^{flox/flox}$;Villin-Cre mice and $K8^{flox/flox}$;Villin-$CreER^{t2}$ mice in the C57BL/6 background ($K8^{flox/flox}$ mice generated by Karen Ridge, Northwestern University; Stenvall *et al.*, 2021) were bred and genotyped by PCR as previously described (Baribault *et al.*, 1994; Stenvall *et al.*, 2021). All animals were housed at the Central Animal Laboratory of the University of Turku and treated according to animal study protocols (no. 197/04.10.07/2013, no. 3956/04.10.07/2016, and no. ESAVI/16359/2019) approved by the State Provincial Office of South Finland. The mice were killed by CO_2 inhalation and tissue samples were collected. Pieces of the proximal colon (PC) and distal colon (DC) were collected for protein and RNA analysis and immunofluorescence staining. Colon epithelium was collected for protein and

RNA analysis by scraping the luminal side of the colon with a chilled glass slide as previously described (Helenius *et al.*, 2015). Ileum, liver, pancreas, and lungs were collected for protein analysis. Protein analysis of colon epithelium and PC were performed on samples from 2–5-mo-old male and female mice unless otherwise stated. Pancreas were collected from 2–3-mo-old male and female mice, lungs were collected from 8–10.5-mo-old male and female mice, and liver and ileum were collected from 5.5–6.5-mo-old male and female mice. $K8^{flox/flox}$;Villin-Cre mice and $K8^{flox/flox}$;Villin-Cre-ER^{t2} mice in the C57BL/6 background were of mixed gender and 4–7 mo of age (Stenvall *et al.*, 2021). LAP2$\alpha^{-/-}$ mice were in the C57BL/6 background and 3–3.5 mo old. Spleen and colon were collected from 5–6-mo-old $Vim^{+/+}$ and $Vim^{-/-}$ mice in the C57BL/6 background.

Tamoxifen treatment of mice

A 15 mg/ml solution of tamoxifen (Sigma Aldrich, CA) was prepared by dissolving 30 mg tamoxifen in 2 ml corn oil (Sigma Aldrich, CA). $K8^{flox/flox}$;Villin-$CreER^{t2}$ mice received an intraperitoneal injection with 100 µl of either tamoxifen (1.5 mg tamoxifen/mouse) or vehicle solution (corn oil) once per day for 5 consecutive days, whereafter the mice were kept for 3.5 weeks before they were sacrificed. For the time-course experiment, mice received an intraperitoneal injection with 100 µl of either tamoxifen (1.5 mg tamoxifen/mouse) or vehicle solution (corn oil) once per day for 3 consecutive days, whereafter they were sacrificed at different time points between 0 and 14 days.

Antibiotic treatment of mice

Male and female $K8^{+/+}$ and $K8^{-/-}$ mice were treated with the broad-spectrum antibiotic vancomycin and imipenem (Hospira, IL) administered via drinking water (68 mg/kg body weight/day of each antibiotic) for 8 weeks starting at 18-19 days of age, while control mice received normal drinking water. The drinking water (with or without antibiotics) was changed three times a week. Upon completion of the antibiotic treatment, the 2.5-mo-old mice were killed by CO_2 inhalation, and colon epithelium was collected as described above.

DSS treatment of mice

2% DSS (40 kDa; TdB Consultancy AB, Sweden) was administered in autoclaved water to 2.5-mo-old male BALB/c mice for 8 days. Upon completion of the DSS treatment, the mice were killed by CO_2 inhalation and colon total lysate samples were collected.

Cell culture and sustained siRNA treatment with recovery

Caco-2 cells (DSMZ, Braunschweig, Germany) were grown on 10-cm cell culture plates in DMEM containing 10% fetal calf serum, 2 mM L-glutamine, 100 units/ml penicillin, and 100 µg/ml streptomycin. The cells were cultured at 37°C in a 5% CO_2 atmosphere. For siRNA experiments, Caco-2 cells were plated on 24- or 12-well plates so that the cells were 20–30% confluent at the time of siRNA transfection. Caco-2 cells were mock transfected (all reagents except siRNA), transfected with K8/K18 scramble siRNA, or transfected with K8/K18 siRNA (Supplemental Table 1) using Lipofectamine 2000 (Invitrogen, CA) according to the manufacturer's instructions (Strnad *et al.*, 2016). siRNA transfections were performed using 30 or 60 pmol of each siRNA and 1.5 or 3 µl Lipofectamine 2000 per well in 24- or 12-well plates, respectively. For sustained keratin knockdown, siRNA transfections were repeated three times, followed by 72 hours of incubation and subculture after each transfection, and by the end of the third 72-hour incubation samples were collected for protein analysis and immunofluorescence staining. Recovery of cells following siRNA treatment was achieved by incubating previously siRNA-treated cells three times for a 72-hour period, which was followed by subculture. Samples were collected for protein analysis at the end of the third incubation period (9 days after the removal of siRNA).

CRISPR/Cas9-mediated K8 knockout in Caco-2 cells

$K8^{-/-}$ Caco-2 cells were established with lentivectors and CRISPR/Cas9 technology at the Genome Editing Core at the Turku Bioscience Centre (Turku, Finland). A two-component CRISPR system was used to generate K8 knockout cells (Adli, 2018). Single guide RNAs (sgRNAs) for K8 (Supplemental Table 2) were designed using the Chopchop tool and cloned according to the Feng Zhang lab protocol.

Generation of lentiviruses

Separate lentivectors containing spCas9 (lentiCas9-Blast; a gift from Feng Zhang (Broad Institute of MIT and Harvard, Cambridge, MA); Addgene plasmid #52962) and sgRNA (lentiGuide-Puro; a gift from Feng Zhang; Addgene plasmid #52963) were produced in the 293FT packaging cell line by transient cotransfection. In short, on the day of transfection, 50–60% confluent HEK 293FT cells grown on 10-cm dishes were transfected with 14 µg of transfer vector, 4 µg of packaging vector psPAX2 (a gift from Didier Trono, School of Life Sciences, Ecole Polytechnique Fédérale de Lausanne, Lausanne, Switzerland; Addgene plasmid #12260) and 2 µg envelope vector pMD2.G (a gift from Didier Trono; Addgene plasmid #12259) using the $CaCl_2$ method. The DNA-HeBS mix was incubated for 30 min at room temperature before adding to the cells. After overnight incubation the medium with DNA precipitate was gently removed from the cells and replaced with fresh full medium. Media containing viral particles was collected after 72 hours, centrifuged at 300 rpm for 5 min at room temperature to remove cell debris, filtered through a 0.45-µm PES filter, and concentrated by ultracentrifugation for 2 hours at 25,000 rpm at 4°C. At least ten 10-cm dishes were prepared for each vector. The pellet containing lentiviral particles was suspended in the residual medium, incubated for ~2 hours at 4°C with occasional mild vortexing, aliquoted, snap-frozen, and stored at –70°C. The lentiviral titer was determined using a P24 ELISA assay according to the manufacturer's instructions.

Generation of K8 knockout Caco-2 cells

To generate $K8^{-/-}$ clones in Caco-2 cells, 100,000 cells were seeded per well on 24-well plates. The next day, cells were transduced with Lenti-Cas9 (MOI 1, 3, 6), and 72 hours later 10 µg/ml blasticidin was applied to select only Cas9-expressing cells. Cells transduced with the smallest amount of Lenti-Cas9 particles that survived selection proceeded to the next step. In the second stage, the mixed pool of cells stably expressing Cas9 was transduced with one of the lenti sgRNA vectors (MOI 6, 9, 12), and 72 hours later 3 µg/ml puromycin was applied to the cells to select Cas9+/Lenti sgRNA+ double-positive cells. Based on Western blot results, the cell populations showing the highest reduction in K8 protein levels were single-cell sorted (Sony SH800 cell sorter; Sony Biotechnology, CA) and regrown into clonal cell populations. Out of the three sgRNAs used for K8 knockout, only sgRNA#1 showed a clear decrease in protein level in a mixed cell population and, after single-cell cloning, gave full $K8^{-/-}$ clones.

Immunoprecipitation

Caco-2 cells from two 10-cm cell culture plates were washed with phosphate-buffered saline (PBS) and harvested by scraping.

Next, the cells were lysed in 1.5 ml lysis buffer (25 mM HEPES, pH 8.0, 100 mM NaCl, 5 mM EDTA, 0.5% Triton X-100, 20 mM β-glycerophosphate, 20 mM para-nitrophenyl phosphate, 100 µM ortovanadate, 0.5 mM phenylmethylsulfonyl fluoride, 1 mM dithiothreitol, and 1X cOmplete mini protease inhibitor cocktail [Roche, Switzerland]), homogenized by passing the cells through a 23G needle 10 times and rested 45 min on ice. For immunoprecipitation, cell lysates were incubated with rabbit anti-lamin A (Abcam, UK) or mouse anti-K18 (L2A1; Bishr Omary, Rutgers University) antibody (not added to control samples) under rotation at 4°C overnight. Protein-A/G magnetic beads (30 µl; Thermo Fisher Scientific, Waltham, MA) were added to each sample and the samples were incubated under rotation at 4°C for 20 min. The samples were washed three times in TEG buffer (20 mM Tris-HCl, pH 7.5, 1 mM EDTA, 10% glycerol, 0.5 mM phenylmethylsulfonyl fluoride, 1 mM dithiothreitol and 1X cOmplete mini protease cocktail; Roche, Switzerland), dissolved in 3X laemmli sample buffer, and analyzed by SDS–PAGE and Western blot.

SDS–PAGE and Western blot

Protein samples were homogenized on ice in homogenization buffer (0.187 M Tris-HCl, pH 6.8, 3% SDS, and 5 mM EDTA) supplemented with 1X cOmplete protease inhibitor cocktail (Roche, Switzerland) and 1 mM phenylmethylsulfonyl fluoride. Sample protein concentrations were determined with a Pierce BCA protein assay kit (Thermo Fisher Scientific, Waltham, MA) and the samples were normalized and diluted to 5 µg protein/10 µl with 3X laemmli sample buffer (30% glycerol, 3% SDS, 0.1875 M Tris-HCl, pH 6.8, 0.015% bromophenol blue, and 3% β-mercaptoethanol). The samples were separated on 6–10% SDS-polyacrylamide gels together with Precision Plus Protein Dual Color Standards (Bio-Rad, CA) or iBright Prestained Protein Ladder (Thermo Fisher Scientific, Waltham, MA), transferred to polyvinylidene fluoride membranes and analyzed by Western blot (primary and secondary antibodies are listed in Supplemental Tables 3 and 4). HRP-labeled proteins were detected with Amersham ECL Western Blotting Detection Reagent (GE Healthcare, UK) or Western Lightning Plus-ECL (Perkin Elmer, MA) and visualized either on SUPER RX x-ray films (Fuji Corporation, Tokyo, Japan) or using an iBright FL1000 imaging system (Invitrogen, CA). Fluorescently labeled proteins were detected using an iBright FL1000 imaging system (Invitrogen, CA). The Western blot results were quantified using ImageJ software (National Institutes of Health, MD; Schneider *et al.*, 2012) and normalized to loading controls (Hsc70 or β-tubulin).

Microarray analysis

Colon epithelium was isolated from 4-mo-old male $K8^{+/+}$ and $K8^{-/-}$ mice as previously described. The isolated colon epithelium was homogenized with a TissueRuptor homogenizer (Qiagen, Germany) and RNA was isolated using a Nucleospin RNA isolation kit (Macherey-Nagel, Germany). Gene expression profiling by microarray and data analysis was performed by the Finnish Functional Genomics Centre at the Turku Bioscience Centre using an Illumina Mouse WG-6 v.2.0 Expression BeadChip (Illumina, CA).

RNA isolation and quantitative RT-PCR

Total lysates of colon tissue were obtained by collecting and combining pieces of PC and DC from 2–5-mo-old $K8^{+/+}$ and $K8^{-/-}$ male and female mice. The samples were homogenized with a TissueRuptor homogenizer (Qiagen, Germany) and RNA was isolated using a Nucleospin RNA isolation kit (Macherey-Nagel, Germany). Agarose gel analysis was used to assess RNA quality. cDNA was synthesized from 1 µg of each RNA sample using Oligo$(dT)_{15}$ Primer (Promega) and M-MLV Reverse Transcriptase (RNase H Minus, Point Mutant; Promega). Quantitative (q)RT-PCR reactions for target genes were prepared using specific primer (Oligomer; Helsinki, Finland or Metabion International, Planegg, Germany) and probe (Universal Probe Library, Roche, Basel, Switzerland) combinations (Supplemental Table 5). The target genes were amplified and detected with an Applied Biosystems QuantStudio 3 Real-Time PCR System (Thermo Fisher Scientific) and the gene expression levels were normalized to *β-Actin*. Each cDNA was amplified in triplicates.

Cryosectioning, fixation, immunofluorescence staining, and imaging

Pieces of PC and DC from 2–5-mo old $K8^{+/+}$ and $K8^{-/-}$ male and female mice were embedded in Tissue-Tek O.C.T. Compound (Sakura Finetek Europe B.V., Alphen aan den Rijn, The Netherlands) and frozen. The samples were sectioned into 6-µm-thick cross sections with a Leica CM3050 S Research Cryostat (Leica Microsystems, Wetzlar, Germany), mounted on microscope slides and fixed with 1% paraformaldehyde (PFA) in PBS, pH 7.4 (Sigma Aldrich, CA) at RT for 10 min. Caco-2 cells were cultured on cover slips and fixed similarly with 1% PFA at RT for 10 min. The fixed tissue sections and cell samples were stained as previously described (Ku *et al.*, 2004). Immunofluorescence staining was performed using the antibodies listed in Supplemental Tables 3 and 4 and counterstained using the nuclear markers DRAQ5 (Cell Signaling, MA) or DAPI (Invitrogen, CA). The samples were mounted with ProLong Gold Antifade (Thermo Fisher Scientific) or VECTASHIELD PLUS (Vector Laboratories, CA). Samples were visualized and imaged at room temperature using a Leica TCS SP5 Matrix confocal microscope (Leica Microsystems) equipped with a 63× Leica PL Apochromat/1.32 oil objective (Leica Microsystems) or a 100× Leica PL Fluotar/1.3 oil objective (Leica Microsystems) using Leica LAS software or a 3i Marianas spinning-disk confocal microscope (Intelligent Imaging Innovations) equipped with a Hamamatsu sCMOS Orca Flash4 v2 C11440-22CU camera (Hamamatsu Photonics, Japan) and a 20× Zeiss Plan-Apochromat/0.8 dry objective (Carl Zeiss AG, Germany) or a 63× Zeiss Plan-Apochromat/1.4 oil objective (Carl Zeiss AG) using Slidebook 6 software. Identical microscopy settings were applied to all samples within one imaging experiment. Images were processed using ImageJ/Fiji (Schindelin *et al.*, 2012; Schneider *et al.*, 2012) and Adobe Photoshop (Adobe, CA) software.

Leptomycin B treatment

Caco-2 cells were cultured on glass cover slips in 24-well plates until 50–60% confluency was reached. The cells were washed with warm PBS, whereafter 1 ml cell media containing 50 nM leptomycin B (LMB; stock solution in 70% ethanol; Cell Signaling) was added to the wells. Control wells got the same amount of ethanol (negative controls) without LMB. The cells were incubated for 6 hours, washed twice with PBS, and fixed with 100% acetone at –20°C for 10 min. The cells were then washed 3 × 5 min with PBS and immunostained as previously described.

Video capture

Fixed and stained Caco-2 cells were captured on a Hamamatsu sCMOS Orca Flash4.0 V2 using a 3i Marianas CSU-W1 spinning-disk confocal microscope using a 100× Zeiss Plan-Apochromat NA 1.4 and Z step size 270 nm. DNA-DAPI was imaged with a 405 nm laser and 445/45 nm filter, lamin A–Alexa 488 imaged with a 488 nm laser and 525/30 nm filter, and Keratin 8–Alexa 568 imaged with a 561 nm

laser and 617/73 nm filter. The image was deconvolved with Scientific Volume Imaging Huygens Essential version 21.04 using a theoretical PSF and the CMLE algorithm, with SNR:12 and max 40 iterations. The video was created using Arivis Vision4D version 3.5.

Hematoxylin & eosin staining

Pieces of PC from 2–5-mo-old male and female mice were fixed with 4% neutral formalin and embedded in paraffin. The samples were sectioned into 4-µm-thick longitudinal sections, mounted on microscope slides and stained using hematoxylin & eosin (H&E). The stained samples were scanned using a Pannoramic 250 slide scanner (3DHISTECH, Budapest, Hungary) with a 20× objective. CaseViewer software (3DHISTECH, software version 2.4) was used for creating images for analysis.

Fluorescence intensity analysis

ImageJ/Fiji was used for quantifying nuclear lamin fluorescence intensity. Cell nuclei were segmented using a fixed mask (default threshold method; threshold range 30–255; dilation using one iteration and one count) that covered both the interior and the nuclear lamina of nuclei in DAPI images. Overlapping nuclei, which could not be segmented, and cell debris were excluded from analysis manually. In addition, only colonocytes lining the colonic crypts were selected for analysis in images of tissue. The mask was overlayed onto lamin A images, and the fluorescence intensity was measured.

Nuclear morphology analysis

ImageJ/Fiji was used for analysis of nuclear morphology parameters. Briefly, cell nuclei were selected for analysis using a fixed mask that segmented nuclei (default threshold method; threshold range 30–165), whereafter poorly segmented and overlapping nuclei were deselected manually. H&E-stained images of PC were further processed by only selecting surface and crypt colonocytes, with the exception of colonocytes in the bottom of the crypts, as they segmented very poorly due to significant overlapping. The morphology of segmented nuclei was analyzed by measuring nuclear area and roundness ($4 * \text{area}/[\pi * \text{major axis}^2]$).

Nuclear integrity analysis

$K8^{+/+}$ and $K8^{-/-}$ Caco-2 cells were grown on glass coverslips in 24-well plates. Upon 30–50% confluence, the cells were transfected with plasmids expressing a nuclear localization signal (NLS) tagged with GFP (NLS-GFP in text; pCDH-NLS-copGFP-EF1-BlastiS was a gift from Jan Lammerding; Addgene plasmid #132772) and the cytoplasmic DNA sensor cGAS tagged with mCherry (cGAS-RFP in text; pCDH-cGAS-E225A D227A-mCherry2-EF1-Puro was a gift from Jan Lammerding, Cornell University; Addgene plasmid #132771; Denais *et al.*, 2016). The transfections were performed with Lipofectamine 2000 according to the manufacturer's instructions using 0.25 µg of each plasmid and 1.75 µl Lipofectamine 2000 per well. After 24 h of incubation, when the cells had reached 70–80% confluence, the medium was replaced with 500 µl DMEM. The cells were exposed to shear stress for 24 h at a rotational rate of 200 rpm in a horizontal orbital shaker (Thermo Fisher Scientific) based on a previously described setup (Driessen *et al.*, 2020). Static control cells were placed in the same incubator as the orbital shaker. After 24 h, all cells were fixed with 1% PFA for 15 min and fluorescence staining of DNA (DAPI), mounting, and imaging were performed as described above. The number of cells with only nucleoplasmic or both nucleoplasmic and cytoplasmic NLS-GFP and cGAS-mCherry in healthy cells was quantified.

Statistical analysis

All quantified Western blot results were statistically analyzed using one way-ANOVA and *t* test in GraphPad Prism 5 (GraphPad Software, CA). The results show the mean ± SD with significant differences shown as * = $p < 0.05$, ** = $p < 0.01$, or *** = $p < 0.001$.

ACKNOWLEDGMENTS

We thank Gerhard Wiche (Max Perutz Labs, University of Vienna) for the kind donation of the plectin antibody, Jan Lammerding (Cornell University) for the plasmids used in nuclear integrity analysis, Cecilia Sahlgren and Freddy Suarez-Rodriguez (Åbo Akademi University [ÅAU]) for assistance with the orbital shaker model, Pekka Taimen (University of Turku) for fruitful discussions, Keijo Viiri (University of Tampere) for the Cre-villin mouse strains, Petra Fichtinger (Max Perutz Labs, Medical University of Vienna) for help with the LAP2α mice, and John Eriksson (Turku Bioscience Centre, University of Turku and ÅAU, and Biosciences/Cell Biology, ÅAU) and members of the Eriksson laboratory, especially Elin Torvaldson and Josef Gullmets, for $vimentin^{-/-}$ mice, reagents, and discussions. We are grateful to all members of the Toivola laboratory, especially Frank Weckström and Molly Feiring (Biosciences/Cell Biology, Faculty of Science and Engineering, Åbo Akademi University; ÅAU). Imaging was performed at the Cell Imaging and Cytometry Core at Turku Bioscience Centre (University of Turku and ÅAU) and Biocenter Finland. This work was financed by the Academy of Finland 140759/126161/332582/315139 (D.M.T.), the InFLAMES Flagship Programme of the Academy of Finland, Sigrid Juselius Foundation (D.M.T.), Turku Doctoral Programme in Molecular Biosciences at ÅAU (C-G.A.S., J.H.N.), Medicinska Understödsföreningen Liv och Hälsa Foundation (D.M.T., J.H.N., C-G.A.S.), EU FP7 IRG (D.M.T.), ÅAU Centers of Excellence of Cell Stress and Molecular Aging and Cellular Mechanostasis (D.M.T.), The Swedish Cultural Foundation in Finland (J.H.N., C-G.A.S.), Makarna Agneta och Carl-Erik Olins Foundation (J.H.N., C-G.A.S.), Victoria Foundation (C-G.A.S., J.H.N.), K. Albin Johansson Foundation (C-G.A.S., J.H.N.), Magnus Ehrnrooths stiftelse (J.H.N.) Kommersrådet Otto A. Malms Donationsfond (J.H.N.), Waldemar von Frenckells Foundation (J.H.N.), the EuroCellNet COST Action (CA15214; D.M.T., R.F.), National Institutes of Health (NIH) PO1 GM-096971 (R.D.G.), and NIH RO-106023 (R.D.G.).

REFERENCES

Adli M (2018). The CRISPR tool kit for genome editing and beyond. Nat Commun 9, 1911.

Almeida FV, Walko G, McMillan JR, McGrath JA, Wiche G, Barber AH, Connelly JT (2015). The cytolinker plectin regulates nuclear mechanotransduction in keratinocytes. J Cell Sci 128, 4475–4486.

Ameen NA, Figueroa Y, Salas PJ (2001). Anomalous apical plasma membrane phenotype in CK8-deficient mice indicates a novel role for intermediate filaments in the polarization of simple epithelia. J Cell Sci 114, 563–575.

Asghar MN, Priyamvada S, Nyström JH, Anbazhagan AN, Dudeja PK, Toivola DM (2016). Keratin 8 knockdown leads to loss of the chloride transporter DRA in the colon. Am J Physiol Gastrointest Liver Physiol 310, G1147–G1154.

Asghar MN, Silvander JS, Helenius TO, Lähdeniemi IA, Alam C, Fortelius LE, Holmsten RO, Toivola DM (2015). The amount of keratins matters for stress protection of the colonic epithelium. PLoS One 10, e0127436.

Baribault H, Penner J, Iozzo RV, Wilson-Heiner M (1994). Colorectal hyperplasia and inflammation in keratin 8-deficient FVB/N mice. Genes Dev 8, 2964–2973.

Belt EJ, Fijneman RJ, van den Berg EG, Bril H, Delis-van Diemen PM, Tijssen M, van Essen HF, de Lange-de Klerk ES, Belien JA, Stockmann HB, *et al.* (2011). Loss of lamin A/C expression in stage II and III colon cancer is associated with disease recurrence. Eur J Cancer 47, 1837–1845.

Brady GF, Kwan R, Bragazzi Cunha J, Elenbaas JS, Omary MB (2018). Lamins and lamin-associated proteins in gastrointestinal health and disease. Gastroenterology 154, 1602–1619.e1601.
Chen NY, Kim P, Weston TA, Edillo L, Tu Y, Fong LG, Young SG (2018). Fibroblasts lacking nuclear lamins do not have nuclear blebs or protrusions but nevertheless have frequent nuclear membrane ruptures. Proc Natl Acad Sci USA 115, 10100–10105.
Coulombe PA, Hutton ME, Letai A, Hebert A, Paller AS, Fuchs E (1991). Point mutations in human keratin 14 genes of epidermolysis bullosa simplex patients: genetic and functional analyses. Cell 66, 1301–1311.
Coulombe PA, Omary MB (2002). 'Hard' and 'soft' principles defining the structure, function and regulation of keratin intermediate filaments. Curr Opin Cell Biol 14, 110–122.
Crisp M, Liu Q, Roux K, Rattner JB, Shanahan C, Burke B, Stahl PD, Hodzic D (2006). Coupling of the nucleus and cytoplasm: role of the LINC complex. J Cell Biol 172, 41–53.
Dechat T, Adam SA, Taimen P, Shimi T, Goldman RD (2010). Nuclear lamins. Cold Spring Harb Perspect Biol 2, a000547.
Dechat T, Pfleghaar K, Sengupta K, Shimi T, Shumaker DK, Solimando L, Goldman RD (2008). Nuclear lamins: major factors in the structural organization and function of the nucleus and chromatin. Genes Dev 22, 832–853.
de Leeuw R, Gruenbaum Y, Medalia O (2018). Nuclear lamins: thin filaments with major functions. Trends Cell Biol 28, 34–45.
Denais CM, Gilbert RM, Isermann P, McGregor AL, te Lindert M, Weigelin B, Davidson PM, Friedl P, Wolf K, Lammerding J (2016). Nuclear envelope rupture and repair during cancer cell migration. Science 352, 353–358.
Driessen R, Zhao F, Hofmann S, Bouten C, Sahlgren C, Stassen O (2020). Computational characterization of the dish-in-a-dish, a high yield culture platform for endothelial shear stress studies on the orbital shaker. Micromachines 11, 552.
Escobar-Hoyos LF, Shah R, Roa-Pena L, Vanner EA, Najafian N, Banach A, Nielsen E, Al-Khalil R, Akalin A, Talmage D, Shroyer KR (2015). Keratin-17 promotes p27KIP1 nuclear export and degradation and offers potential prognostic utility. Cancer Res 75, 3650–3662.
Flint Brodsly N, Bitman-Lotan E, Boico O, Shafat A, Monastirioti M, Gessler M, Delidakis C, Rincon-Arano H, Orian A (2019). The transcription factor Hey and nuclear lamins specify and maintain cell identity. eLife 8, e44745.
Flitney EW, Kuczmarski ER, Adam SA, Goldman RD (2009). Insights into the mechanical properties of epithelial cells: the effects of shear stress on the assembly and remodeling of keratin intermediate filaments. FASEB J 23, 2110–2119.
Gesson K, Vidak S, Foisner R (2014). Lamina-associated polypeptide (LAP)2α and nucleoplasmic lamins in adult stem cell regulation and disease. Semin Cell Dev Biol 29, 116–124.
Habtezion A, Toivola DM, Asghar MN, Kronmal GS, Brooks JD, Butcher EC, Omary MB (2011). Absence of keratin 8 confers a paradoxical microflora-dependent resistance to apoptosis in the colon. Proc Natl Acad Sci USA 108, 1445–1450.
Habtezion A, Toivola DM, Butcher EC, Omary MB (2005). Keratin-8-deficient mice develop chronic spontaneous Th2 colitis amenable to antibiotic treatment. J Cell Sci 118, 1971–1980.
Heffler J, Shah PP, Robison P, Phyo S, Veliz K, Uchida K, Bogush A, Rhoades J, Jain R, Prosser BL (2020). A balance between intermediate filaments and microtubules maintains nuclear architecture in the cardiomyocyte. Circ Res 126, e10–e26.
Helenius TO, Misiorek JO, Nyström JH, Fortelius LE, Habtezion A, Liao J, Asghar MN, Zhang H, Azhar S, Omary MB, Toivola DM (2015). Keratin 8 absence down-regulates colonocyte HMGCS2 and modulates colonic ketogenesis and energy metabolism. Mol Biol Cell 26, 2298–2310.
Hobbs RP, DePianto DJ, Jacob JT, Han MC, Chung BM, Batazzi AS, Poll BG, Guo Y, Han J, Ong S, *et al*. (2015). Keratin-dependent regulation of Aire and gene expression in skin tumor keratinocytes. Nat Genet 47, 933–938.
Jacob JT, Nair RR, Poll BG, Pineda CM, Hobbs RP, Matunis MJ, Coulombe PA (2020). Keratin 17 regulates nuclear morphology and chromatin organization. J Cell Sci 133, jcs254094.
Jiang H, Xue X, Panda S, Kawale A, Hooy RM, Liang F, Sohn J, Sung P, Gekara NO (2019). Chromatin-bound cGAS is an inhibitor of DNA repair and hence accelerates genome destabilization and cell death. EMBO J 38, e102718.
Ketema M, Kreft M, Secades P, Janssen H, Sonnenberg A (2013). Nesprin-3 connects plectin and vimentin to the nuclear envelope of Sertoli cells but is not required for Sertoli cell function in spermatogenesis. Mol Biol Cell 24, 2454–2466.
Ketema M, Wilhelmsen K, Kuikman I, Janssen H, Hodzic D, Sonnenberg A (2007). Requirements for the localization of nesprin-3 at the nuclear envelope and its interaction with plectin. J Cell Sci 120, 3384–3394.
Krndija D, El Marjou F, Guirao B, Richon S, Leroy O, Bellaiche Y, Hannezo E, Matic Vignjevic D (2019). Active cell migration is critical for steady-state epithelial turnover in the gut. Science 365, 705–710.
Ku NO, Darling JM, Krams SM, Esquivel CO, Keeffe EB, Sibley RK, Lee YM, Wright TL, Omary MB (2003). Keratin 8 and 18 mutations are risk factors for developing liver disease of multiple etiologies. Proc Natl Acad Sci USA 100, 6063–6068.
Ku NO, Toivola DM, Zhou Q, Tao GZ, Zhong B, Omary MB (2004). Studying simple epithelial keratins in cells and tissues. Methods Cell Biol 78, 489–517.
Kumeta M, Hirai Y, Yoshimura SH, Horigome T, Takeyasu K (2013). Antibody-based analysis reveals "filamentous vs. non-filamentous" and "cytoplasmic vs. nuclear" crosstalk of cytoskeletal proteins. Exp Cell Res 319, 3226–3237.
Lähdeniemi IAK, Misiorek JO, Antila CJM, Landor SK, Stenvall CA, Fortelius LE, Bergström LK, Sahlgren C, Toivola DM (2017). Keratins regulate colonic epithelial cell differentiation through the Notch1 signalling pathway. Cell Death Differ 24, 984–996.
Lee CH, Kim MS, Chung BM, Leahy DJ, Coulombe PA (2012). Structural basis for heteromeric assembly and perinuclear organization of keratin filaments. Nat Struct Mol Biol 19, 707–715.
Libotte T, Zaim H, Abraham S, Padmakumar VC, Schneider M, Lu W, Munck M, Hutchison C, Wehnert M, Fahrenkrog B, *et al*. (2005). Lamin A/C-dependent localization of Nesprin-2, a giant scaffolder at the nuclear envelope. Mol Biol Cell 16, 3411–3424.
Liu C, Liu ED, Meng YX, Dong XM, Bi YL, Wu HW, Jin YC, Zhao K, Li JJ, Yu M, *et al*. (2017). Keratin 8 reduces colonic permeability and maintains gut microbiota homeostasis, protecting against colitis and colitis-associated tumorigenesis. Oncotarget 8, 96774–96790.
Lombardi ML, Lammerding J (2011). Keeping the LINC: the importance of nucleocytoskeletal coupling in intracellular force transmission and cellular function. Biochem Soc Trans 39, 1729–1734.
Misiorek JO, Lahdeniemi IAK, Nystrom JH, Paramonov VM, Gullmets JA, Saarento H, Rivero-Muller A, Husoy T, Taimen P, Toivola DM (2016). Keratin 8-deletion induced colitis predisposes to murine colorectal cancer enforced by the inflammasome and IL-22 pathway. Carcinogenesis 37, 777–786.
Muchir A, Wu W, Worman HJ (2009). Reduced expression of A-type lamins and emerin activates extracellular signal-regulated kinase in cultured cells. Biochim Biophys Acta 1792, 75–81.
Naetar N, Ferraioli S, Foisner R (2017). Lamins in the nuclear interior—life outside the lamina. J Cell Sci 130, 2087–2096.
Naetar N, Korbei B, Kozlov S, Kerenyi MA, Dorner D, Kral R, Gotic I, Fuchs P, Cohen TV, Bittner R, *et al*. (2008). Loss of nucleoplasmic LAP2α–lamin A complexes causes erythroid and epidermal progenitor hyperproliferation. Nat Cell Biol 10, 1341–1348.
Omary MB (2017). Intermediate filament proteins of digestive organs: physiology and pathophysiology. Am J Physiol Gastrointest Liver Physiol 312, G628–G634.
Osmanagic-Myers S, Dechat T, Foisner R (2015). Lamins at the crossroads of mechanosignaling. Genes Dev 29, 225–237.
Patteson AE, Vahabikashi A, Pogoda K, Adam SA, Mandal K, Kittisopikul M, Sivagurunathan S, Goldman A, Goldman RD, Janmey PA (2019). Vimentin protects cells against nuclear rupture and DNA damage during migration. J Cell Biol 218, 4079–4092.
Polari L, Alam CM, Nystrom JH, Heikkila T, Tayyab M, Baghestani S, Toivola DM (2020). Keratin intermediate filaments in the colon: guardians of epithelial homeostasis. Int J Biochem Cell Biol 129, 105878.
Ridge KM, Linz L, Flitney FW, Kuczmarski ER, Chou YH, Omary MB, Sznajder JI, Goldman RD (2005). Keratin 8 phosphorylation by protein kinase C delta regulates shear stress-mediated disassembly of keratin intermediate filaments in alveolar epithelial cells. J Biol Chem 280, 30400–30405.
Schindelin J, Arganda-Carreras I, Frise E, Kaynig V, Longair M, Pietzsch T, Preibisch S, Rueden C, Saalfeld S, Schmid B, *et al*. (2012). Fiji: an open-source platform for biological-image analysis. Nat Methods 9, 676–682.
Schneider CA, Rasband WS, Eliceiri KW (2012). NIH Image to ImageJ: 25 years of image analysis. Nat Methods 9, 671–675.
Schweizer J, Bowden PE, Coulombe PA, Langbein L, Lane EB, Magin TM, Maltais L, Omary MB, Parry DA, Rogers MA, Wright MW (2006). New consensus nomenclature for mammalian keratins. J Cell Biol 174, 169–174.

Shin JY, Worman HJ (2022). Molecular pathology of laminopathies. Annu Rev Pathol 17, 159–180.
Sivaramakrishnan S, Schneider JL, Sitikov A, Goldman RD, Ridge KM (2009). Shear stress induced reorganization of the keratin intermediate filament network requires phosphorylation by protein kinase C zeta. Mol Biol Cell 20, 2755–2765.
Stenvall CA, Tayyab M, Gronroos TJ, Ilomaki MA, Viiri K, Ridge KM, Polari L, Toivola DM (2021). Targeted deletion of keratin 8 in intestinal epithelial cells disrupts tissue integrity and predisposes to tumorigenesis in the colon. Cell Mol Life Sci 79, 10.
Strnad P, Guldiken N, Helenius TO, Misiorek JO, Nystrom JH, Lahdeniemi IA, Silvander JS, Kuscuoglu D, Toivola DM (2016). Simple epithelial keratins. Methods Enzymol 568, 351–388.
Swift J, Ivanovska IL, Buxboim A, Harada T, Dingal PC, Pinter J, Pajerowski JD, Spinler KR, Shin JW, Tewari M, *et al*. (2013). Nuclear lamin-A scales with tissue stiffness and enhances matrix-directed differentiation. Science 341, 1240104.
Tapley EC, Starr DA (2013). Connecting the nucleus to the cytoskeleton by SUN-KASH bridges across the nuclear envelope. Curr Opin Cell Biol 25, 57–62.
Toivola DM, Boor P, Alam C, Strnad P (2015). Keratins in health and disease. Curr Opin Cell Biol 32, 73–81.
Toivola DM, Krishnan S, Binder HJ, Singh SK, Omary MB (2004). Keratins modulate colonocyte electrolyte transport via protein mistargeting. J Cell Biol 164, 911–921.
Toivola DM, Tao GZ, Habtezion A, Liao J, Omary MB (2005). Cellular integrity plus: organelle-related and protein-targeting functions of intermediate filaments. Trends Cell Biol 15, 608–617.
Vahabikashi A, Sivagurunathan S, Nicdao FAS, Han YL, Park CY, Kittisopikul M, Wong X, Tran JR, Gundersen GG, Reddy KL, *et al*. (2022). Nuclear lamin isoforms differentially contribute to LINC complex-dependent nucleocytoskeletal coupling and whole-cell mechanics. Proc Natl Acad Sci USA 119, e2121816119.
Vaughan A, Alvarez-Reyes M, Bridger JM, Broers JL, Ramaekers FC, Wehnert M, Morris GE, Whitfield WGF, Hutchison CJ (2001). Both emerin and lamin C depend on lamin A for localization at the nuclear envelope. J Cell Sci 114, 2577–2590.
Vidak S, Georgiou K, Fichtinger P, Naetar N, Dechat T, Foisner R (2018). Nucleoplasmic lamins define growth-regulating functions of lamina-associated polypeptide 2α in progeria cells. J Cell Sci 131, jcs208462.
Wagner N, Krohne G (2007). LEM-domain proteins: new insights into lamin-interacting proteins. Int Rev Cytol 261, 1–46.
Wallace L, Roberts-Thompson L, Reichelt J (2012). Deletion of K1/K10 does not impair epidermal stratification but affects desmosomal structure and nuclear integrity. J Cell Sci 125, 1750–1758.
Wang AS, Kozlov SV, Stewart CL, Horn HF (2015). Tissue specific loss of A-type lamins in the gastrointestinal epithelium can enhance polyp size. Differentiation 89, 11–21.
Wang L, Mohanasundaram P, Lindstrom M, Asghar MN, Sultana G, Misiorek JO, Jiu Y, Chen H, Chen Z, Toivola DM, *et al*. (2022). Vimentin suppresses inflammation and tumorigenesis in the mouse intestine. Front Cell Dev Biol 10, 862237.
Wilhelmsen K, Litjens SH, Kuikman I, Tshimbalanga N, Janssen H, van den Bout I, Raymond K, Sonnenberg A (2005). Nesprin-3, a novel outer nuclear membrane protein, associates with the cytoskeletal linker protein plectin. J Cell Biol 171, 799–810.
Wilson KL, Foisner R (2010). Lamin-binding proteins. Cold Spring Harb Perspect Biol 2, a000554.
Zhou Q, Toivola DM, Feng N, Greenberg HB, Franke WW, Omary MB (2003). Keratin 20 helps maintain intermediate filament organization in intestinal epithelia. Mol Biol Cell 14, 2959–2971.